Arabian Journal of Chemistry (2020) 13, 3429–3439

King Saud University

Arabian Journal of Chemistry

www.ksu.edu.sa
www.sciencedirect.com

ORIGINAL ARTICLE

Preparation, characterization and performance evaluation of supported zeolite on porous glass hollow fiber for desalination application

Siti Nurfatin Nadhirah Mohd Makhtar [a], Mohamad Zahir Mohd Pauzi [a], Nizar Mu'ammar Mahpoz [a], Norfazilah Muhamad [a], Mukhlis A. Rahman [a,*], Khairul Hamimah Abas [b], Azian Abd Aziz [c], Mohd Hafiz Dzarfan Othman [a], Juhana Jaafar [a]

[a] *Advanced Membrane Technology Research Centre (AMTEC), Universiti Teknologi Malaysia, 81310 Skudai, Johor, Malaysia*
[b] *Faculty of Electrical Engineering, Universiti Teknologi Malaysia, 81310 Skudai, Johor, Malaysia*
[c] *Language Academy, Universiti Teknologi Malaysia, 81310 Skudai, Johor, Malaysia*

Received 13 September 2018; accepted 18 November 2018
Available online 24 November 2018

KEYWORDS

Zeolite;
reverse osmosis (RO);
Sweeping liquid;
Osmotic pressure driven;
In-situ hydrothermal;
Porous glass

Abstract A-type zeolite membranes were synthesized on porous glass hollow fibers that prepared using the in-situ hydrothermal process. The porous glass hollow fibers were prepared using the phase inversion and sintering technique with the addition of yttria stabilized zirconia (YSZ) to improve their porosity. The glass hollow fibers were characterized using the scanning electron microscope (SEM), Fourier transform infrared (FTIR), mechanical properties and water permeability. The porosities of pure glass hollow fiber were improved by the addition of YSZ particles, which lead to an increase in the pure water permeability. The water permeability shows that the glass hollow fiber prepared form spinning suspension E, which has 30 wt% zeolite particles and 20 wt% YSZ particles, has the highest permeability of 155.65 L m^{-2} hr^{-1} bar^{-1} compared to the previous work, which was only 4.0 L m^{-2} hr^{-1} bar^{-1}. This glass hollow fiber was later used as the support for the incorporation of zeolite membrane for the desalination application. The performance of membranes is separating sodium chloride (NaCl) salt solution were tested using two different setups, namely pressure driven reverse osmosis (RO) and sweeping liquid assisted reverse

* Corresponding author.
E-mail address: r-mukhlis@utm.my (M.A. Rahman).
Peer review under responsibility of King Saud University.

Production and hosting by Elsevier

https://doi.org/10.1016/j.arabjc.2018.11.015

osmosis (SLRO). The solute flux for 5,000 and 10,000 ppm NaCl salt solutions were 24.45 and 17.86 L m^{-2} hr^{-1}, respectively. Both operations enabled the solute rejection up to 98%.

1. Introduction

Seawater desalination has been regarded as promising technology, which can overcome fresh water deficit worldwide. To recover pure water from this source, reverse osmosis has been widely adopted. Reverse osmosis has become a current practice in desalination technologies, with water recovery reported to be ranging from 30% to 35% (McCutchen et al., 2006). Polymeric membranes have been used widely for desalination, but there is a growing interest to replace them with ceramic membranes. Among ceramic materials, zeolite has been regarded as the promising material for seawater desalination. Zeolite membranes have been shown to have an excellence performance for ion removal from aqueous solutions by reverse osmosis (RO) processes (Kumakiri, 2000; Li et al., 2004; Jiang et al., 2017). Xu et al. reported that zeolite membranes enabled a selectivity of 10,000 when the membranes were used to purify water from organic solution (Xu et al., 2004). Kumakiri et al. reported that zeolite membrane (with pore size ≈ 0.4 nm) enabled 44% rejection of ethanol/water mixtures with water flux of 0.058 kg m^{-2} h^{-1} (Kumakiri, 2000). Li et al., 2004 demonstrated RO separation using α-alumina-supported MFI-type zeolite membranes for various salt solutions. The results show that the zeolite membranes have a great potential in RO desalination due to their excellent performance in terms of chemical and thermal stabilities (Li et al., 2004).

Zeolite is commonly prepared using hydrothermal crystallization, in-situ hydrothermal synthesis, vapor phase transport, sol gel method, chemical growth, galvanic metal deposition, leakage-blocked method, seeding method (embedding zeolite microcrystal into a support) and microwave synthesis (Kumakiri, 2000; Aoki et al., 1998; Chen et al., 2011; Dong and Long, 2000). Typically, hydrothermal synthesis is used to prepare zeolite on a porous support for membrane-based separation. This approach will produce a thin dense layer of zeolite membrane that enables high water permeability (Kumakiri, 2000). However, if the synthesis process is not controlled properly, thick and loose zeolite layers will be produced. This situation will reduce the performance of zeolite membrane. There was an effort to produce unsupported zeolite membrane using the phase inversion and sintering technique, with the spinneret orifice of 3.2/0.5 mm (OD/ID), extrusion rate of 10 mL/min, air gap of 15 cm, tap water as internal and external coagulants and sintered at temperature ranging from 600 °C to 1400 °C (Nurfatin Makhtar et al., 2017). This established method has been successfully produced various types of ceramic membranes for various applications (Li et al., 2017; Zhu et al., 2017, Abdullah et al., 2016). However, the results showed that the zeolite particles melted during the sintering process at high temperatures. The work also reported that at an intermediate sintering temperature, i.e. 1000 °C, zeolite membrane transformed into a glass membrane. The glass hollow fiber membrane had pure water permeability of 4.0 L m^{-2} h^{-1} bar^{-1} and 85% rejection of bovine serum albumin (BSA), which can be considered insufficient for desalination (Makhtar et al., 2017).

Therefore, this work focused on the development of porous glass hollow fiber, onto which zeolite membranes were deposited using in-situ hydrothermal synthesis. Zeolite particles were extruded into a hollow fiber configuration using the phase inversion and sintering technique. To improve its porosity, yttria stabilized zirconia (YSZ) particles were be added into ceramic suspension prior to the extrusion process. The phase inversion process enabled the glass hollow fiber to be produced in a simpler way with better control in terms of morphology compared to the conventional technique of glass membrane fabrication (Nurfatin et al., 2017). Incorporation of YSZ particles enhanced the mechanical properties of the glass hollow fiber, as this ceramic material is well known for its toughness. The separation performances of the zeolite membranes were tested using two different set-ups of reverse osmosis (RO) system i.e, pressure-driven RO and RO assisted sweep liquid. Water permeability and rejection of salts, i.e. sodium chloride (NaCl) were carried out to examine the performance of the zeolite membrane on the porous glass hollow fiber.

2. Experiments

2.1. Materials

Zeolite (5A) was purchased from Sigma Aldrich (USA), and used as the precursor of the glass membrane. The zeolite particles were pre-dried at 60 °C overnight before ceramic suspension preparation. Commercially available yttria-stabilized zirconia (YSZ) with particle size of 0.3 μm (d_{50} = 0.3 μm), purchased from Fuel Cell Material, used as ceramic particles to be mixed with the zeolite particles. Radel A300 polyethersulfone (PESf) was purchased from Ameco Performance, USA. Polyethyleneglycol 30-dipolyhydroxystrearate, (Arlacel P135) was provided by CRODA Inc. N-methylpyrrolidone (NMP) was purchased from QREC, New Zealand. Sodium aluminate (Na_2AlO_3) and sodium trisilicate ($Na_2O_7Si_3$) was purchased from Sigma Aldrich, which were served as the sources of alumina and silica, respectively. Sodium hydroxide (NaOH) was purchased from Emsure, Darmstadt, Germany. These chemicals were used as received without further treatment.

2.2. Preparation of porous glass hollow fiber

Porous glass hollow fibers were prepared using the phase inversion based spinning technique. 1 wt% of Arlacel P135 was dissolved in NMP prior to the addition of zeolite and YSZ particles. The compositions of spinning suspensions and their sample designation are shown in Table 1. The suspensions were milled using various sizes of milling balls made from alumina, (20 mm and 10 mm) in a planetary ball-milling machine (NQM-2 Planetary Ball Mill). The rate of the plane-

Table 1 Composition of spinning suspension for preparing glass hollow fibers.

Sample Designation	Zeolite composition (wt.%)	Zirconia composition (wt.%)	PESf composition (wt.%)	Solvent composition (wt.%)
A	50.00	0.00	8.33	40.67
B	45.00	5.00	8.33	40.67
C	40.00	10.00	8.33	40.67
D	35.00	15.00	8.33	40.67
E	30.00	20.00	8.33	40.67

tary ball-milling machine was fixed at 182 rpm for 48 h. A polymer binder was added at a fixed ratio of zeolite/YSZ and PESf at 6:1. The milling then was milled for another 48 h. The suspension was extruded using a 3.2/0.5 mm (OD/ID) orifice spinneret to form a hollow fiber precursor. Both internal and external coagulants were tap water. The rate of the extrusion was fixed at 10 mL/min, with the air gap of 15 cm. The hollow fiber precursor was further immersed in tap water for 24 h to complete the phase inversion process and straightened. The straighten precursors were dried before being cut into 35-cm long.

A sintering process took place in a tubular furnace (XY-1700, China). The sintering process was run by gradually increasing the temperature to the final temperature. The sintering temperature was first heated up at 400 °C at a rate of 3 °C min^{-1} for 1 h to completely remove polymer binder. Later, the temperature was further increased to 800 °C at 4 °C.min^{-1}, held for 2 h. This stage was to ensure the burnt-off of the polymer and allowing only zeolite in the membrane. Final sintering temperatures were varied ranging from 1000 to 1200 °C at a heating rate of 5 °C min^{-1}, held for 8 h. The final step of sintering enabled the ceramic particles to grow into larger grains. Finally, the temperature was cooling down to room temperature at rate of 5 °C.min^{-1}.

2.3. In-situ synthesis of zeolite on glass hollow fiber

Zeolite precursor was prepared by dissolving 4.43 g sodium hydroxide (NaOH) in distilled water and divided into two equal volumes. An amount of 4.23 g sodium aluminate and 6.7 g sodium trisilicate were dissolved in separated NaOH solutions. The silica solution was poured drop-wise into a sodium aluminate solution under vigorous stirring. The final solutions were poured into a Teflon-bottle contained porous glass hollow fibers. The hydrothermal synthesis was carried out by placing the Teflon bottle in an oven at 120 °C for 24 h. The membrane obtained was washed by distilled water and dried.

2.4. Performance tests of zeolite membrane supported on glass hollow fiber

The pressure driven reverse osmosis system was developed using the cross-flow filtration mode, shown in Fig. 1a. The feed solution was pumped into the shell side of the membrane module. The permeate flow was collected at the lumen side of the hollow fiber membranes. Salt solutions, with different concentrations, were used as a feed solution. The system was operated with a feed velocity of 10.5 mL s^{-1} and trans-membrane pressure difference of 7 bars(g) at a room temperature. The feed solution was continuously supplied to the hollow fiber modules for 30 min for initial stabilization prior to the collection of permeate for sampling. The pure water permeation was calculated using Eq. (1)

$$J_w = \frac{V}{t \times A \times P} \quad (1)$$

where, J_W (L/m^{-2}.hr^{-1}.bar^{-1}) is pure water permeation, t is time (s), A is the total surface area of hollow fibre membrane (m^2) and P is operating pressure (bar). The rejection of salt was determined by the final concentration of salt permeate which was analysed by ion conductivity meter (Eutech Cond 6+, Thermo Scientific). The salt rejection was calculated using Eq. (2):

$$\%\ \text{Rejection} = \frac{C_i - C_o}{C_i} \times 100 \quad (2)$$

where, C_i is the concentration of salt solution at feed solution and Co is the concentrations of salt solution at permeate.

The RO assisted sweeping liquid was carried out in a membrane module shown in Fig. 1b. The membrane was potted at both ends without closing the lumen of the membrane. Sweeping liquid and the salt solutions were both flowed in a perpendicular closed loop. The salt solution was flowed on the outer surface of zeolite membrane whereas the sweeping liquid was flowed into the lumen of the glass hollow fiber. Variable speed peristaltic pumps were used to pump the liquids. Changes in the weights of both solutions were monitored using weighing balances (Smith). Solute flux was calculated using Eq. (3):

$$J_w = \frac{(m/\rho)}{t \times A} \quad (3)$$

where, J_W (L.m^{-2}.hr^{-1}) is pure water permeation, m is the mass of water permeated through the membrane (kg), ρ (kg.m^3) is density, t is time (s) and A is the total surface area of hollow fibre membrane (m^2). The rejection was determined by measuring the salt solution using an ion conductivity meter (Eutech Cond 6+, Thermo Scientific) at the both salt solution and sweeping liquid at the initial and final process. The rejection was calculated using Eq. (4) (Kumakiri, 2000):

$$R = 1 - \frac{C_{sl}}{C_{salt}} \quad (4)$$

where, R (%) is the rejection, C_{sl} is the concentration of seeping liquid and C_{salt} is the concentrations of salt solution.

2.5. Characterizations

The rheology of the zeolite suspensions was examined using a viscometer (BROOK FIELD) at shear rate extending from 1 to 100 s^{-1}. The test was done before the spinning process using spindle S21. The porous glass hollow fiber membranes

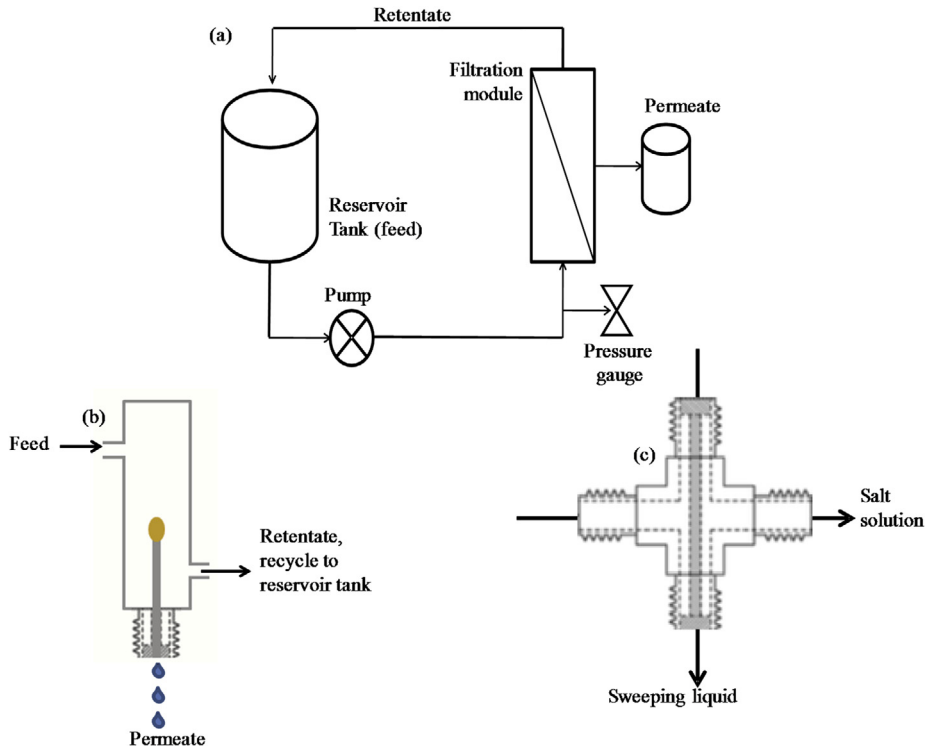

Fig. 1 (a) Filtration system schematic diagram of (b) cross-flow filtration, and (c) sweep liquid assisted filtration.

mechanical strength was acquired by utilizing the three-point bending test (INSTRON-5544) with 1 kN load cell. The mechanical strengths of the membranes were calculated by using Eq. (5).

$$\sigma_F = 8FLD_o/\pi\left(D_o^4 - D_i^4\right) \quad (5)$$

where F is the maximum load, L is the length of the span (43 mm), D_o is the hollow fiber outer diameter and D_i is the hollow fiber inner diameter. The cross-sectional images of glass hollow fibers were acquired utilizing the SEM (TM 3000 HITACHI). The membranes were snapped into 3 mm length and set on a metal holder. The SEM samples were fully covered by a gold/platinum mixture under vacuum for 3 min at 20 mA. X-ray diffraction (XRD) analyses of the membrane were carried out using Philips PW1710 at scan rate of 1°/s, ranging from 3° to 50°. The membrane samples were finely grounded and mounted on a special plat holder before the analysis. The diffraction patterns were used to determine particles sized and crystallinity index using Eq. (6) and (7), respectively.

$$D_p = K\lambda/(B\cos\theta) \quad (6)$$

where D_p (nm) is the crystallite size, K = 0.94 is the Scherrer constant that represent cubic crystallite shape, λ (Å) is the X-ray wavelength, B is the full width at half maximum of the XRD peak and θ is the XRD peak position, one half of 2θ.

$$CI = (I_{NaA}/I_{am})x100\% \quad (7)$$

where CI is the relative degree of crystallinity, I_{NaA} is the relative intensity for the synthesized NaA zeolite and I_{am} is the relatively intensity of as-synthesized NaA amorphous state.

Fourier transform infrared (FTIR) was used to verify the transformation of zeolite into amorphous glass. FTIR analyses were implemented using the Perkin Elmer Spectrum100 (MA, USA). The spectrum was recorded ranging from 650 to 4000 cm^{-1} regions. The repetition of the scanning process was fixed at 32 times.

3. Results and discussion

3.1. Microstructural analysis of modified glass hollow fiber

The zeolite suspensions were spun using a constant extrusion rate of 10 mL min^{-1}, bore fluid of 9 mL min^{-1}, and an air gap of 15 cm, as reported by the previous work. The hollow fiber precursors were later sintered at 1000 °C for 8 h. The cross-sectional images of the glass hollow fibers were acquired using the SEM analysis as shown in Fig. 2. The figures show overall cross sections and the area near to the lumen of glass hollow fibers spun using the ceramic suspensions of A, C, D, and E. The glass hollow fibers prepared using the phase inversion have circular shapes, which directly influenced by viscosity of the ceramic suspensions. The SEM images also show the glass hollow fibers have a number of voids, due to water used as coagulant, trapped in the cross-section during the phase inversion process. This phenomenon can be associated with the ability of zeolite to adsorb water. These SEM images revealed that an increase in the amount of YSZ particles improved their dispersion in zeolite suspensions. At low amount, YSZ particles tended to agglomerate (the sphere shapes in C and D) thus affecting the rheology of ceramic suspensions. It is recommended that minimum amount of YSZ particles should be fixed at 20 wt% (the sphere shapes

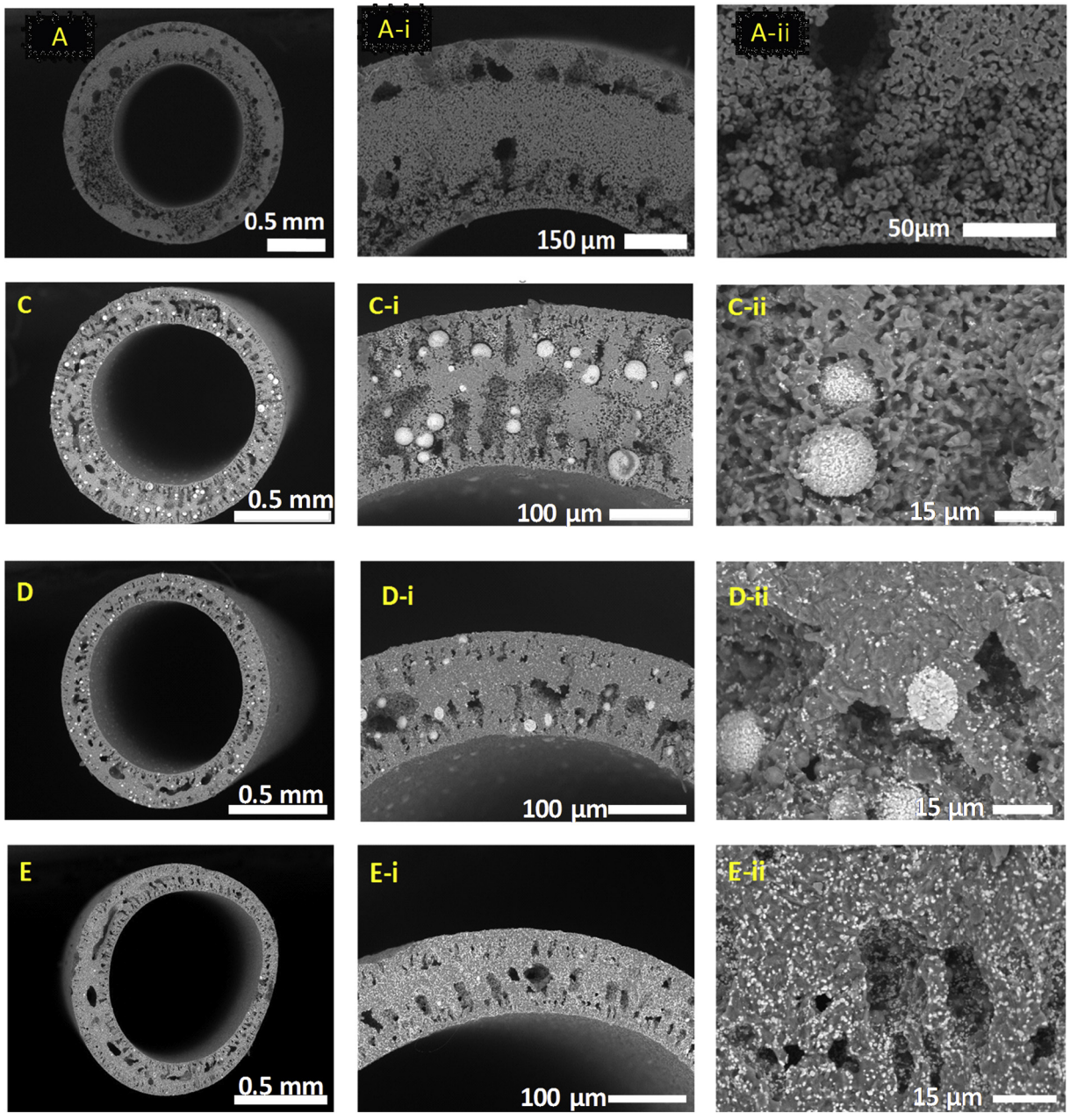

Fig. 2 SEM images of the cross-sectional glass hollow fiber membranes at different magnifications, prepared using zeolite/zirconia loading of (A) 50/0 wt%, (C) 40/10 wt%, (D) 35/15 wt%, and (E) 30/20 wt%, extruded at 10 mL min^{-1}, an air gap of 15 cm with bore fluid at 9 mL min^{-1} and sintered at 1000 °C.

disappear in E) when the total 50 wt% ceramic loading was used to prepare the precursor of glass hollow fiber. The EDX elemental mapping of fiber E was shown in Fig. 3. A well-dispersed pattern of zirconia (Zr), silica (Si) and alumina (Al) were observed.

3.2. Chemical and porosity analysis of porous glass hollow fiber

Fig. 4 shows the FTIR spectra for zeolite, YSZ and glass hollow fiber prepared from ceramic suspension C (40/10 wt%), D (35/15 wt%), and E (30/20 wt%). The appearance of pure zeolite was confirmed by the presence of peaks at 713, 972, 1647 and 3286 cm^{-1} whereas YSZ was characterized by the presence of peaks at 1362, 1515 and 3442 cm^{-1}. Low intensity peaks at the 1346 and 1515 cm^{-1} bands associated to symmetric and asymmetric stretching vibrations of the carboxylate groups. Peak at 3442 cm^{-1} represents the asymmetric vibrational frequency of the Zr—OH (Alexander et al., 2015; Palenta et al., 2015; Shameli et al., 2011; Razavi et al., 2015; Zhang et al., 2004). An increase in the amount of zeolite over YSZ particles caused in the reduction of peaks at 972 cm^{-1}, which represented by the vibration of overlapping symmetric and asymmetric of T—O bond, where T is Si or Al, i.e. Si—O or Al—O. The reduction in the peak intensity showed the

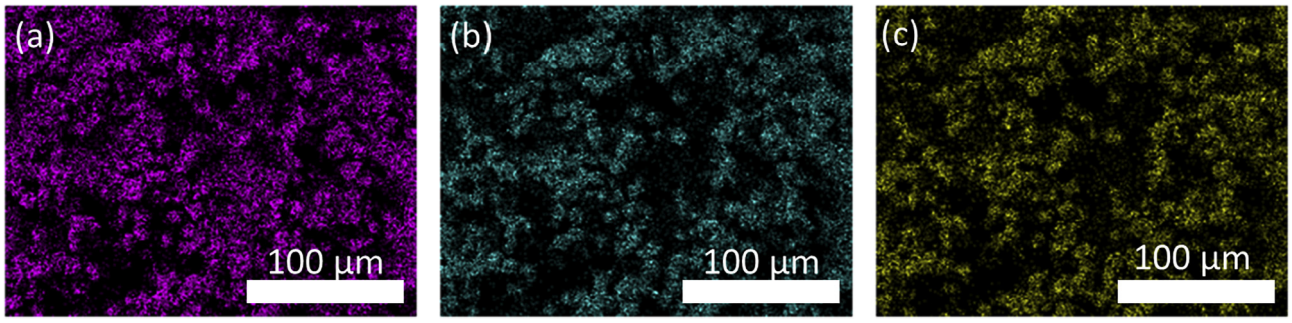

Fig. 3 EDX elemental mapping of (a) Zr, (b) Si and (c) Al of glass hollow fiber prepared using zeolite/YSZ at 30/20 wt% sintered at 1000 °C.

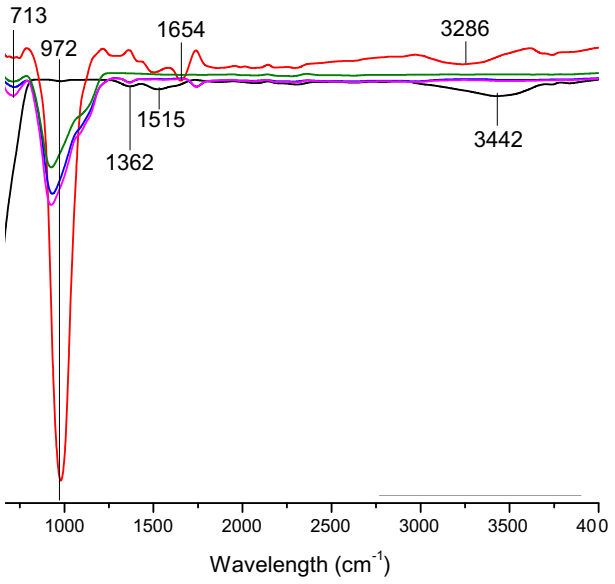

Fig. 4 Ex-situ infrared spectra of zeolite (—), YSZ (—) and glass membrane prepared from ceramic suspension C (—), D (—), and, E (—), sintered at 1000 °C.

disappearance of Si—O or Al—O bonds, which might be caused by the formation of Si—O—Zr or Al—O—Zr linkages. However, the absence of new peak indicated that no chemical interaction occurred between zeolite and YSZ particles.

Fig. 5(a) shows the diffraction pattern of sample E, prepared using zeolite/YSZ at 30/20 wt%. Both amorphous and crystalline phases were observed in the data. The amorphous phase indicated that zeolite have completely transformed to glass phase, while the crystalline phase, observed at peaks 30°, 35°, 50° and 60° were attributed to YSZ particles (Xu et al., 2004). The results obtained from mercury porosimetry analysis, as shown in Fig. 5(b), show the addition of YSZ particles affected the average porosity of glass hollow fiber during its initial preparation step. Addition of 10 wt% of YSZ particles caused the formation of large voids (1801 nm), due to particle agglomeration. Further adding the YSZ particles to 20 wt % facilitated in reducing the size of voids (514 nm), as the YSZ particles of 30/20 wt% (E) dispersed uniformly in the matrix of the glass hollow fiber.

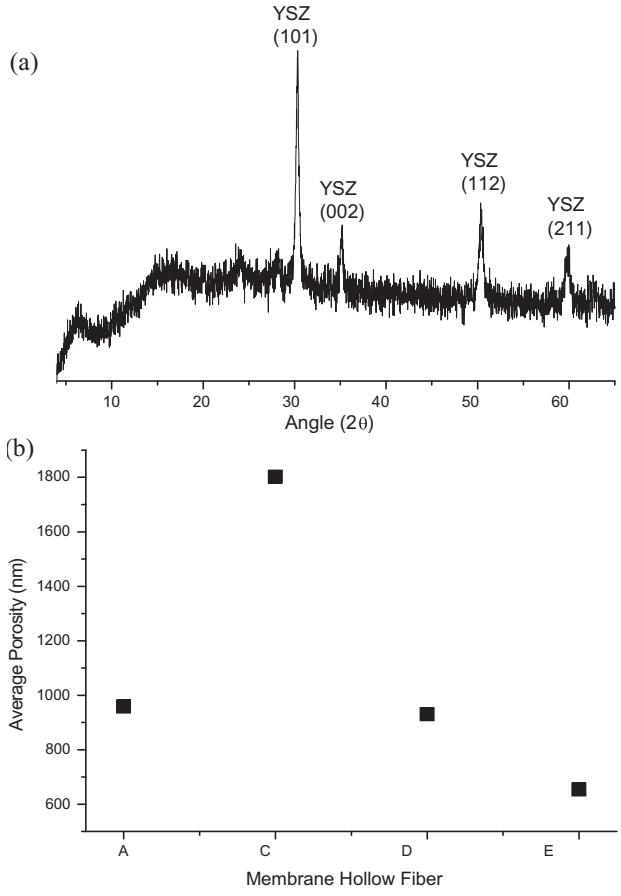

Fig. 5 (a) XRD pattern of glass hollow fiber prepared using zeolite/YSZ at 30/20 wt% sintered at 1000 °C and (b) average porosity of glass hollow fibers prepared using ceramic suspensions of (A) 50/0 wt%, (C) 40/10 wt%, (D) 35/15 wt%, and (E) 30/20 wt%, extruded at 10 mL min^{-1}, an air gap of 15 cm with bore fluid at 9 mL min^{-1} The porosity values were obtained using the mercury porosimetry analysis (Pascal 140).

3.3. Mechanical properties of glass hollow fiber

The effect of ceramic loadings on the mechanical properties of the glass hollow fiber was studied at a constant extrusion rate of 10 mL min^{-1}, bore fluid of 9 mL min^{-1}, and an air gap of

15 cm. Fig. 6 shows the mechanical properties of the glass hollow fiber, sintered at temperature ranging from 1000 to 1200 °C, using the triple bending point tests. The highest mechanical strength of the glass hollow fiber was 36.68 ± 3.57 MPa, prepared using ceramic suspension of D, which contain 30 wt% of zeolite and 20 wt% of YSZ, and sintered at 1000 °C. The mechanical strength of the glass hollow fiber was affected by the addition of YSZ particles. Differences in the mechanical strength between pure glass hollow fibers with its composite were caused by the difference in the grain size and the coefficient of thermal expansion (CTE) of glass and YSZ particles. Densification occurred during the sintering process caused a neck growth between the ceramic particles, which created physical bonds between the particles. Surface diffusion happened during the sintering process caused the development of the neck between the glass particles, and simultaneously formed a bond between the other particles to increase the mechanical strength (Paiman et al., 2015; Bouzera et al., 2006; Tan et al., 2010). However, a contradict trend was observed when YSZ was added. A decrease in the mechanical strength was observed with an increase in the YSZ particles. It is expected that the difference in the co-efficient of thermal expansion (CTE) between glass and YSZ particles caused the difference in the densification rate during the sintering process. The negative CTE value for glass particles and positive CTE value for YSZ particles prevented the neck growing, thus creates a void between zeolite and YSZ granules (Biswas et al., 2011; Yamashita et al., 2017; Carey et al., 2014). As these granules become bigger, the void between zeolite and YSZ also become bigger. This caused a reduction in the mechanical strength when the sintering temperature was increased from 1000 °C to 1200 °C.

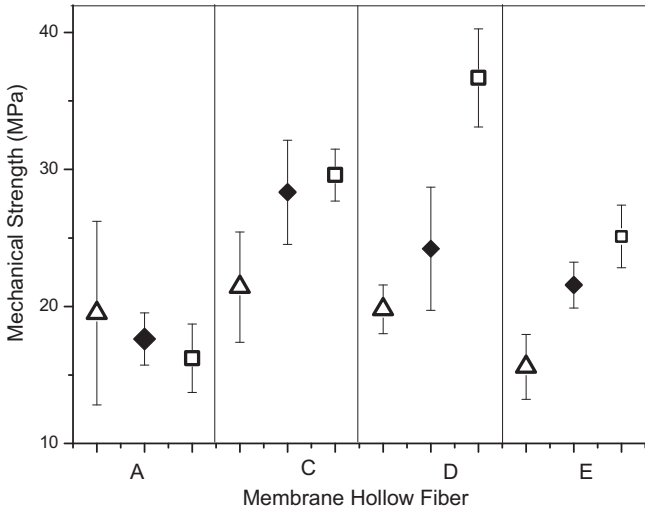

Fig. 6 Mechanical strength of glass hollow fiber membranes prepared using zeolite/YSZ loading of (A) 50/0 wt%, (C) 40/10 wt %, (D) 35/15 wt%, and (E) 30/20 wt%, extruded at 10 mL min^{-1}, an air gap of 15 cm with bore fluid at 9 mL min^{-1} and sintered at 1200 °C (Δ), 1100 °C (◆), and 1000 °C (□).

3.4. Permeability of porous glass hollow fiber

Water permeabilities of the glass hollow fibers were studied using a cross-flow system operated at 2 bars. Fig. 7 shows the pure water permeabilities through glass hollow fibers prepared using ceramic suspension of C, D, and E. The results show that the glass hollow fibers prepared using the phase inversion and sintering technique yielded water permeabilities ranging from 2.6 to 155.65 L m^{-2} hr^{-1} bar^{-1}. An increase in the permeability of the glass hollow fibers was observed as the sintering temperature was reduced. This trend was expected as the membrane structures were densified as the temperature increased. This may cause further hindrance to the water pathways across the membranes. The highest permeation was obtained from glass hollow fibers prepared using ceramic suspensions of E, which contain 30 wt% zeolite and 20 wt% YSZ, and sintered at 1000 °C. An addition of the YSZ particles enabled an increase in the pure water permeability of the glass hollow fibers. Although this data seem to

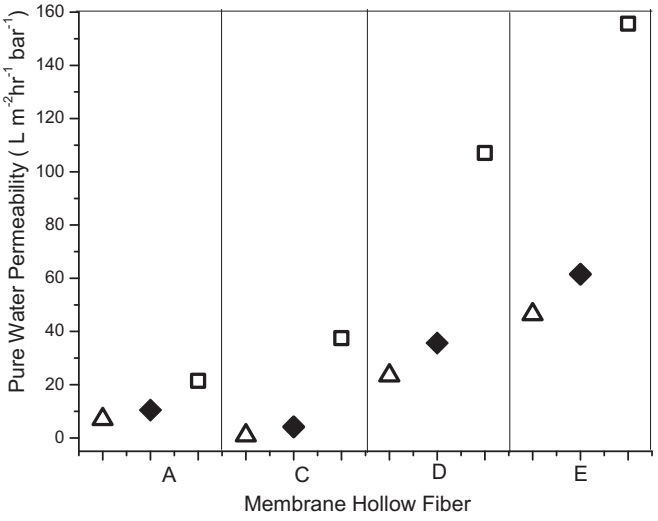

Fig. 7 Permeability of pure water for glass hollow fibers prepared using ceramic suspensions of (A) 50/0 wt%, (C) 40/10 wt%, (D) 35/15 wt%, and (E) 30/20 wt%, extruded at 10 mL min^{-1}, an air gap of 15 cm with bore fluid at 9 mL min^{-1} and sintered at 1200 °C (Δ), 1100 °C (◇), and 1000 °C (□).

contradict with the average porosity reported in Fig. 5b, the agglomeration of YSZ particles, at lower YSZ percentage, i.e. 10 wt%, caused the glass hollow fiber to possess permeability similar to glass hollow fiber. When the amount of YSZ particles was increased, dispersion occurred uniformly that led to higher surface area to facilitate water permeation. The agglomeration may cause high average porosity of glass hollow fiber but the region that did not have enough YSZ particles tended to become dense, due to glass transformation, thus reducing water permeability.

3.5. Incorporation of zeolite particles on porous glass hollow fiber

The addition of YSZ particles into glass hollow fiber has been shown to increase its permeability, but it may reduce solute rejection greatly due to the presence of porous structure. To improve any solute rejection, zeolite deposition on outer surface of the glass hollow fiber was proposed. It is expected that using glass as an inert support may contribute to better adhesion due to the similarity of the chemical composition between these two inorganic materials. Zeolite prepared on the glass hollow fiber, synthesized at 120 for 12 h was characterized using the XRD analysis. The result of the synthesized NaA zeolite can be observed in Fig. 8. To confirm its originality, the data was then compared with XRD zeolite data from International Zeolite Association (IZA) for Linde Type A (Treacy, 2001). The XRD pattern obtained in this work was identical with LTA phase identification from Joint Committee of Powder Diffraction Standards (JCPDS) file no 97-002-4901 (Jiang et al., 2017). It was found that the peak positions were slightly different from the database indicating a slight difference in the zeolite NaA chemical structure (Aoki et al., 1998), however, zeolite NaA main characteristic are clearly visible, suggesting that the particle on the glass hollow fiber was NaA zeolite. The zeolite NaA was expected to co-exist with zeolite NaX, which supported by the presence of additional diffraction peaks other than the zeolite NaA (Xu et al., 2001). The shape of XRD peaks (high intensity and broad peaks) indicated that the zeolite prepared in this work was in

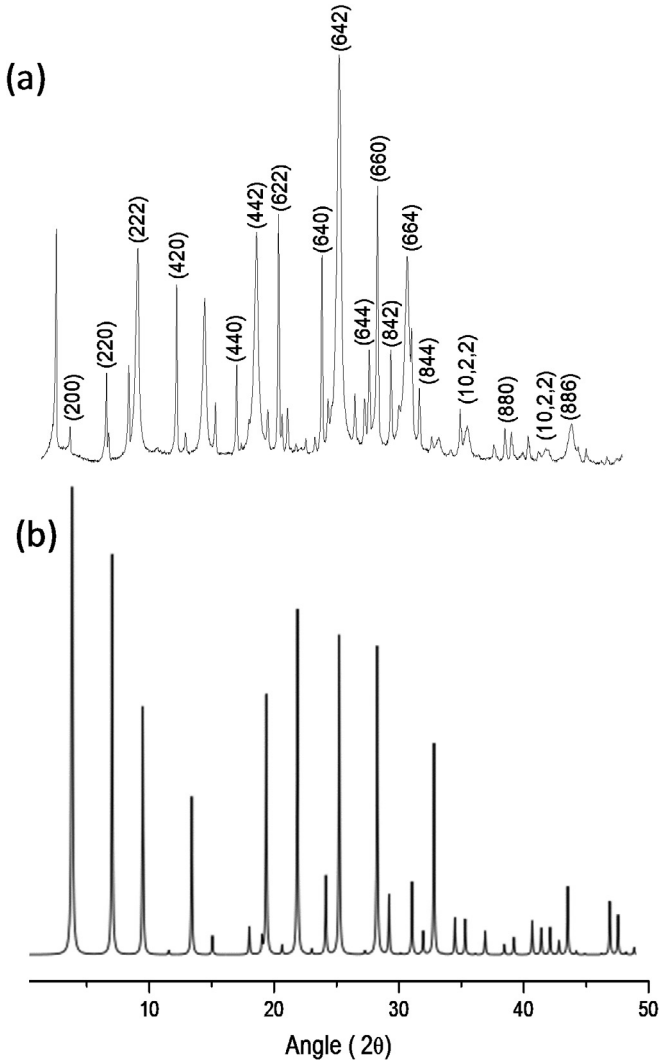

Fig. 8 XRD peaks for (a) zeolite prepared using the hydrothermal method, synthesis for 12 h at 120 °C and (b) zeolite data from International Zeolite Association (IZA) for Linde Type A.

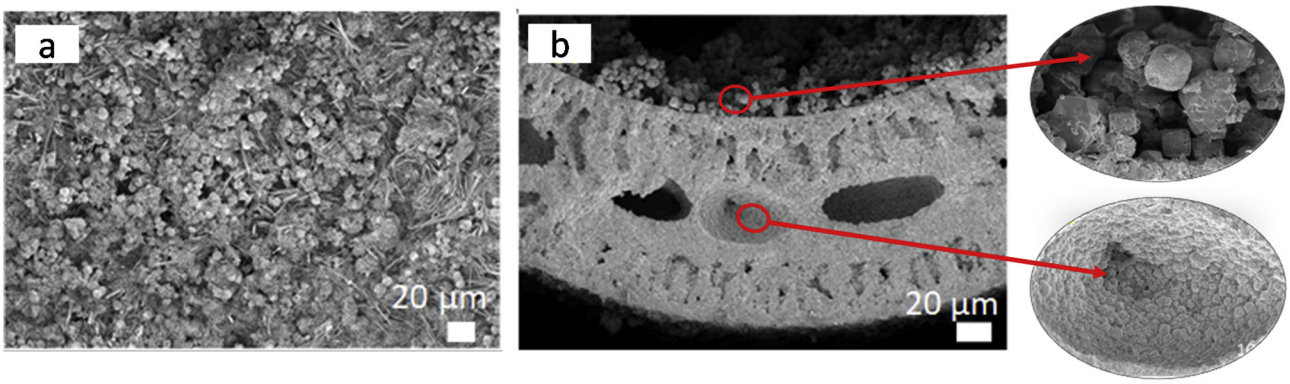

Fig. 9 FESEM images for (a) outer surface and (b) cross-section of porous glass hollow fiber membranes. Inserted images show the difference in particle size between zeolite particles grew on the lumen and the void surface.

the form of nano-sized crystal. Based on the Scherrer equation, the zeolite has particles size of approximately 1.84 nm using the peak at 28.2° with the crystallinity index of 88.14%.

Fig. 9 shows the FESEM images of zeolite membrane synthesized on the glass hollow fiber using the hydrothermal process. Fig. 9(a) shows that the zeolite membrane on the outer surface of glass hollow fiber, whereas Fig. 9(b) shows the cross-section of glass hollow fiber after zeolite deposition. These figures suggested that zeolite deposition could occur at entire surface of glass hollow fiber as long as the surface has the direct contact with the mother solution used in the hydrothermal process. Glass surface with better access to the mother solution has bigger zeolite grains compared to surface that has minimal access to mother solution, i.e., zeolite particles in the lumen and outer surface of glass hollow fiber have bigger grains compared to zeolite particles grew in the voids of glass hollow fiber. The effects of zeolite incorporation on glass hollow fiber were investigated through its porosity using N_2 adsorption of BJH model as shows in Fig. 10. Two different peaks positions at 2.0–5.0 nm and 10–20 nm was observed. Peak 2.0–5.0 nm may attribute to the void between the particles while peak at 10–20 nm may attributed due to the void between the agglomeration particles as illustrated in Fig. 10.

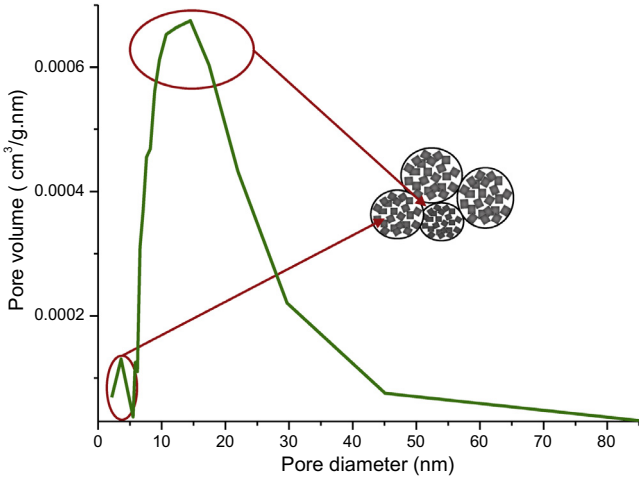

Fig. 10 BJH pore size distribution plot of N_2 adsorption on zeolite NaA, with the pores probability illustration of the matching peaks.

3.6. Performance of supported zeolite on porous glass hollow fiber for salt removal

The performance of zeolite membrane supported on the porous glass hollow fiber was evaluated based on its capability to remove NaCl. The separation process was carried out under 7 bar(g) feed-side pressure at a room temperature using salt solutions with 5,000 and 10,000 ppm concentrations. The preliminary result of desalination using porous glass hollow fiber showed insignificant salt rejection of 17% and solute flux of 5.15 L $m^{-2}hr^{-1}$ (7 bar(g)). The salt rejection and solute flux of zeolite membrane on the porous glass hollows were shown in Fig. 11. It was found that the solute flux of 5,000 and 10,000 ppm of NaCl are 2.65 L m^{-2} hr^{-1} with the rejection of 83.1% and 1.56 L m^{-2} hr^{-1} with the rejection of 83.5% respectively. An increase in the solute concentration from 5,000 ppm to 10,000 ppm caused the solute flux to drop as higher concentration of solute caused hindrance to water diffusion. These results are comparable to the study reported by Zhu et al. The author found out that only 0.03 L m^{-2} h^{-1} of

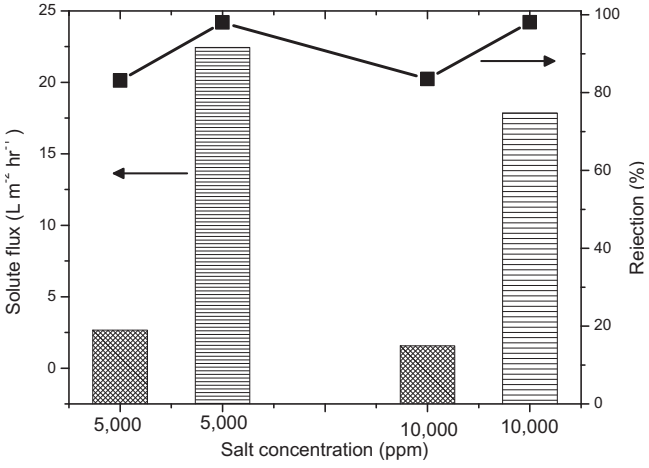

Fig. 11 Water permeability of RO-NaCl (▒), SLRO-NaCl (▒) for zeolite membranes, prepared using in-situ hydrothermal method for 12 h at 120 °C.

water flux, and 0.02 L m^{-2} h^{-1} of solute flux, with the rejection of more than 93.0% was obtained from seawater under the applied pressure of 700 kPa (7 bar) for 180 days using MFI type zeolite membrane (Zhu et al., 2014).

Fig. 11 also shows the solute flux and rejection of the zeolite membrane tested using different configuration namely sweeping liquid reverse osmosis (SLRO). Using this system, no pressure was applied in the feed but the solute flux was collected by the assistance of sweeping liquid flowed at high volumetric flow rate through the lumen. The process is inspired by the Bernoulli's principle that stated that the pressure is increased by decreasing the fluid flow rate. SLRO system was taking advantages of the hollow fiber configuration itself to provide maximum surface contact between lumen and outer surface. In this study, NaCl salt solution was introduced on the outer surface of zeolite hollow fiber membrane, which is the active layer (zeolite), whereas the sweeping liquid (deionized water) was introduced through the lumen of the hollow fiber. The flow rate of the salt solution was slower (125 mL/min) than the flow rate of the sweep liquid solution (248 mL/min), to enable the pressure difference between the salt solution and the sweep liquid solution based on the Bernoulli's principle. Fig. 11 shows solute flux for both 5,000 and 10,000 ppm NaCl salt solutions were of 24.45 and 17.86 L m^{-2} hr^{-1}, respectively. An increase in the permeability suggested that the changing in the water permeation configuration could significantly improve the performance of the membrane. The water from the salt solution was forced to permeate into the lumen of the hollow fiber due to the high flow rate that crease low-pressure environment in the lumen of hollow fiber. The membrane enabled a rejection up to 98% for both 5,000 and 10,000 ppm NaCl salt solutions.

4. Conclusion

At loading of 20 wt%, the addition of YSZ particles was able to improve the water permeability. FTIR result showed that YSZ particles were not chemically bonded to the glass hollow fiber but the mechanical strength of glass hollow fibers were significantly improved. The highest permeability was found using the suspension E which has 30% zeolite particles and 20% YSZ particles. The glass hollow fiber then was successfully incorporated with zeolite particles using the in-situ hydrothermal method at 120 °C for 12 h. The performance of zeolite membrane was tested via water permeation and rejection of salt by reverse osmosis (RO) and sweeping liquid assisted reverse osmosis (SLRO). It was found that SLRO improved greatly the water permeation and rejection. The solute flux for 5,000 and 10,000 ppm NaCl salt solutions were 24.45 and 17.86 L m^{-2} hr^{-1}, respectively. Both operations enabled the solute rejection up to 98%.

Acknowledgement

The authors gratefully acknowledge financial support from various parties, namely, the Malaysia Ministry of Higher Education (MOHE) through FRGS (0.J130000.7823.4F947), the Higher Institution Centre of Excellence (HICoE) Research Grant (R. J090301.7846.4 J178), and Universiti Teknologi Malaysia (UTM) through the Research University grant (Q.J130000.2546.16H34, Q.J130000.2446.04G30). Appreciation also goes to UTM Research Management Centre for both financial and technical support.

References

Abdullah, N., Rahman, M.A., Ha, M., Othman, D., Ismail, A.F., Jaafar, J., Abd, A., 2016. Preparation and characterization of self-cleaning alumina hollow Fi Ber membrane using the phase inversion and sintering technique lumen structure. Ceramics Int. 42, 12312–12322.

Alexander, S., Morrow, L., Lord, A.M., Dunnill, C.W., Barron, A.R., 2015. PH-responsive octylamine coupling modification of carboxylated aluminium oxide surfaces. J. Mater. Chem. A 3 (18), 10052–10059.

Aoki, K., Kusakabe, K., Morooka, S., 1998. Gas permeation properties of A-type zeolite membrane formed on porous substrate by hydrothermal synthesis. J. Membr. Sci. 141, 197–205.

Biswas, M., Kumbhar, C.S., Gowtam, D.S., 2011.. Characterization of Nanocrystalline Yttria-Stabilized Zirconia : An In Situ HTXRD Study. ISRN Nanotechnol. 2011.

Bouzerara, F., Harabi, A., Achour, S., Larbot, A., 2006. Porous ceramic supports for membranes prepared from kaolin and doloma mixtures. J. European Ceram. Soc. 26, 1663–1671.

Carey, T., Tang, C.C., Hriljac, J.A., Anderson, P.A., 2014. Chemical control of thermal expansion in cation-exchanged zeolite. Chem. Mater.

Chen, H., Wydra, J., Zhang, X., Lee, P., Wang, Z., Fan, W., Tsapatsis, M., 2011. Hydrothermal synthesis of zeolites with three-dimensionally ordered mesoporous-imprinted structure. J. American Chem. Soc., 12390–12393

Dong, W., Long, Y., 2000. Preparation of an MFI-type zeolite membrane on a porous glass disc by substrate self-transformation. Chem. Commun. 2, 1067–1068.

Jiang, J., Wang, X., Peng, L., Wang, X., Gu, X., 2017. Microporous and mesoporous materials batch-scale preparation of hollow Fi Ber supported CHA zeolite membranes and module for solvents dehydration. Micropor. Mesopor. Mater. 250, 18–26.

Kumakiri, I., Yamaguchi, T., Nakao, S.I., 2000. Application of a zeolite a membrane to reverse osmosis process. J. Chem. Eng. Japan 33 (2), 333–336. Pdf.

Li, L., Dong, J., Nenoff, T.M., Lee, R., 2004. Desalination by reverse osmosis using MFI zeolite membranes. J. Membr. Sci. 243, 401–404.

Li, T., Lu, X., Wang, B., Wu, Z., Li, K., Brett, D.J.L., Shearing, P.R., December 2016. X-Ray tomography-assisted study of a phase inversion process in ceramic hollow Fi Ber systems – towards practical structural design. J. Memb. Sci. 2017 (528), 24–33. December.

McCutcheon, J.R., McGinnis, R.L., Elimelech, M., 2006. Desalination by ammonia-carbon dioxide forward osmosis: influence of draw and feed solution concentrations on process performance. J. Memb. Sci. 278 (1–2), 114–123.

Nurfatin, S., Mohd, N., Rahman, M.A., 2017. Preparation and characterization of glass hollow fiber membrane for water. Purific. Appl.

Paiman, S.H., Rahman, M.a., Othman, M.H.D., Ismail, a.F., Jaafar, J., Aziz, A.A., 2015. Morphological study of yttria-stabilized zirconia hollow fibre membrane prepared using phase inversion/sintering technique. Ceram. Int. 41 (10), 12543–12553.

Palenta, T., Fuhrmann, S., Greaves, G.N., Schwieger, W., Wondraczek, L., 2015. Thermal collapse and hierarchy of polymorphs in a faujasite-type zeolite and its analogous melt-quenched glass. J. Chem. Phys. 142 (8), 084503.

Science, S., Razavi, R.S., View, G., 2015. Synthesis and characterization of non- transformable tetragonal YSZ nanopowder by means of pechini method for ... synthesis and characterization of non-

transformable tetragonal coatings (TBCs) applications. J. Sol-gel Sci. Technol. No. September.

Shameli, K., Ahmad, M.Bin., Zargar, M., Yunus, W.M.Z.W., Ibrahim, N.A., 2011. Fabrication of silver nanoparticles doped in the zeolite framework and antibacterial activity. Int. J. Nanomed. 6, 331–341.

Tan, X., Wang, Z., Li, K., 2010. Fiber membranes. Ind. Eng. Chem. Res., 2895–2901

Treacy, M. M. J. Collection of Simulated XRD Powder Patterns for Zeolites Editors : 2001.

Xu, X., Yang, W., Liu, J., Lin, L., Stroh, N., Brunner, H., 2004. Synthesis of NaA zeolite membrane on a ceramic hollow fiber. J. Memb. Sci. 229 (1–2), 81–85.

Xu, B.X., Yang, W., Liu, J., Lin, L., 2001. Synthesis of a high permeance NaA zeolite membrane by microwave heating. Sep. Purific. Technol. 25 (1–3), 241–249.

Yamashita, T., Yamazaki, S.; Sato, T.; Matsui, T., Yamashita, T., Yamazaki, S., Sat, T., Matsui, T., 2017. Phase Study and Thermal Expansion of Yttria Stabilized Zirconia Doped with PuO 2-x Phase Study and Thermal Expansion of Yttria Stabilized Zirconia Doped with PU02-X. 3131 (November).

Zhang, Y., Yan, Z., Liao, F., Liao, C., Yan, C.,2004. (RE ¼ Y , Sc) Solid Solutions. (39), 1763–1777.

Zhu, B., Hong, Z., Milne, N., Doherty, C.M., Zou, L., Lin, Y.S., Hill, A.J., Gu, X., Duke, M., 2014. Desalination of seawater ion complexes by MFI-Type zeolite membranes: temperature and long term stability. J. Memb. Sci. 453, 126–135.

Zhu, J., Meng, X., Zhao, J., Jin, Y., Yang, N., Zhang, S., 2017. Facile Hydrogen/nitrogen separation through graphene oxide membranes supported on YSZ ceramic hollow fibers. J. Memb. Sci. 535, 143–150. April.